NOTE

Computation of the optical properties of turbid media from slope and curvature of spatially resolved reflectance curves

Marion Jäger, Florian Foschum and Alwin Kienle

Institut für Lasertechnologien in der Medizin und Meßtechnik, Helmholtzstraße 12, 89081 Ulm, Germany

E-mail: marion.jaeger@ilm.uni-ulm.de

Abstract. The optical properties of turbid media were calculated from the curvature at the radial distance ρ^O and the slope at the radial distance ρ^* of simulated spatially resolved reflectance curves (ρ^O (ρ^*) denotes a decrease of the spatially resolved reflectance curve of 0.75 (2.4) orders of magnitude relative to the reflectance value at 1.2 mm). We found correlations between the curvature at ρ^O and the reduced scattering coefficient as well as the slope at ρ^* and the absorption coefficient. For the determination of the optical properties we used these two correlations. The calculation of the reduced scattering coefficient from the curvature at ρ^O is practically independent from the absorption coefficient. Knowing the reduced scattering coefficient within a certain accuracy allows the determination of the absorption coefficient from the slope at ρ^*. Additionally, we investigated the performance of an artificial neural network for the determination of the optical properties using the above explained correlations. This means we used the derivatives as input data. Our artificial neural network was capable to learn the mapping between the optical properties and the derivatives. In effect, the results for the determined optical properties improved in comparison to the above explained method. Finally, the procedure was compared to an artificial neural network that was trained without using the derivatives.

PACS numbers: 07.05.TP, 07.05.Mh, 78.20.Ci, 87.10.Rt, 87.64.Aa

Keywords: artificial neural network, inverse problem, optical properties, turbid media
Submitted to: *Phys. Med. Biol.*

1. Introduction

The non-invasive determination of the optical properties (OP) of tissue is an important research area and especially relevant for clinical applications. Many techniques for the determination of the OP of tissue are reported in the literature, i.e. Wang *et al* 1994, Kienle *et al* 1996, Pfefer *et al* 2003, Yaqin *et al* 2003, Martelli and Zaccanti 2007,

Warncke *et al* 2009, Wang *et al* 2010, Zhang *et al* 2010, Jäger and Kienle 2011 and Kanick *et al* 2011. For example robust and fast methods such as an artificial neural network (ANN) are investigated for an efficient calculation of the absorption and reduced scattering coefficients. Farrell *et al* 1992 first reported the application of an ANN for the non-invasive determination of the OP of turbid media. They simulated experimental reflectance data using a solution of the diffusion theory. The reflectance data R were plotted using $\ln(\rho^2 \cdot R(\rho))$ with ρ being the radial distance. Correlations between the total optical transport coefficient and the effective attenuation coefficient with the shape of the curve were utilized. Farrell *et al* showed that an ANN is capable of discerning these distinct differences in shape and can be used for the determination of the OP.
In this study, we present a novel method for the determination of the OP of turbid media from simulated spatially resolved reflectance (SRR) data. Correlations between the first and second derivative at a certain radial distance of the SRR curve and the OP serve for a fast determination of the reduced scattering coefficient μ_s' and the absorption coefficient μ_a. For the calculation of μ_s' we used the curvature of the SRR curve at ρ^O (see figure 1a)). Knowing the determined μ_s' within a certain accuracy it is possible to calculate μ_a from the slope of the SRR curve at ρ^* (see figure 1a)). In combination with an ANN the results for the determination of the OP are improved.

2. Correlations between slope and curvature and the optical properties

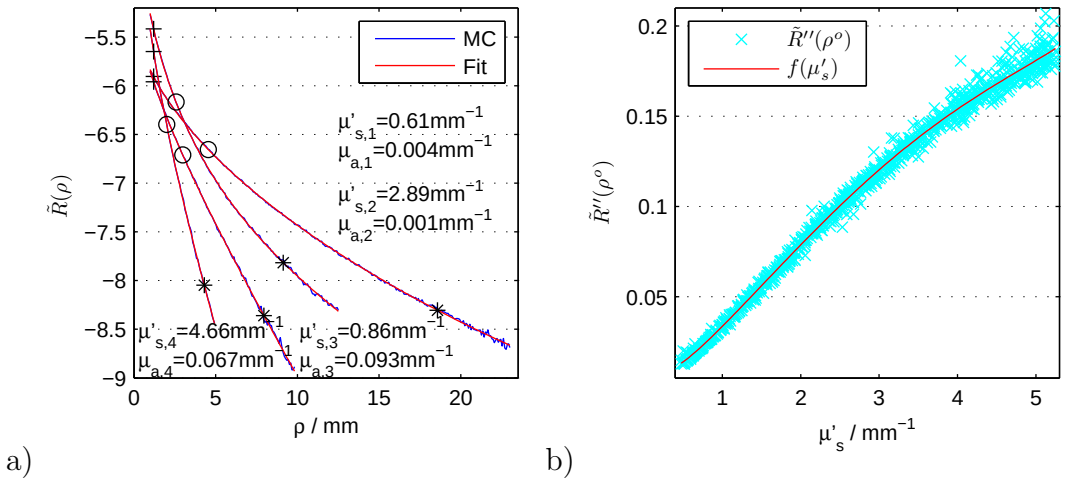

Figure 1. a) Some logarithmic SRR curves and 3 distinct radial distances: The first radial distance ρ^+ is located at $\tilde{R}(1.2\,\text{mm})$, the second at ρ^O, the third at ρ^* where the SRR curve decreased 0.75 and 2.4 orders of magnitude relative to $\tilde{R}(\rho^+)$, respectively. b) Correlation between the reduced scattering coefficient μ_s' and the curvature $\tilde{R}''(\rho^O)$.

Monte Carlo simulations (MC) were performed considering the setup geometry of the experimental arrangement described by Foschum *et al* 2011 (for the MC simulations see also Jäger *et al* 2013). The reduced scattering coefficient was randomly chosen out of

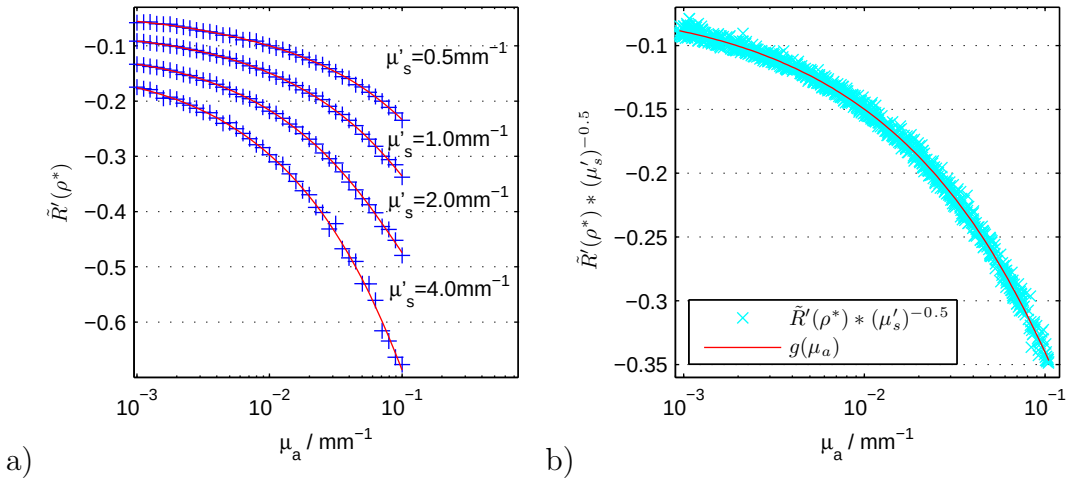

Figure 2. a) Correlation between the absorption coefficient μ_a and the slope $\tilde{R}'(\rho^*)$ (ρ^* see figure 1a)) for different μ_s'. b) Plot for 1000 SRR curves using the known reduced scattering coefficient.

the range $0.475\,\mathrm{mm}^{-1} < \mu_s' < 5.25\,\mathrm{mm}^{-1}$ and the absorption coefficient out of the range $0.00095\,\mathrm{mm}^{-1} < \mu_a < 0.105\,\mathrm{mm}^{-1}$. For liquid phantoms consisting of buffer, Intralipid and ink we used the refractive index $n = 1.33$, the anisotropy factor $g = 0.72$ and the phase function of Intralipid. This phase function was measured at 662 nm using a home-build goniometer as explained by Foschum and Kienle 2013. In order to achieve noise comparable to measurement data we used 10^6 photons for $\mu_a < 0.1\,\mathrm{mm}^{-1}$ and $7 \cdot 10^6$ photons for the rest. With the CCD-camera it is possible to measure the SRR curve up to the radial distance $\rho = 23\,\mathrm{mm}$ and over maximal 3 orders of magnitude relative to the reflectance value at $\rho = 1\,\mathrm{mm}$. In the range of $\rho = 1\,\mathrm{mm}$ up to maximal $\rho = 23\,\mathrm{mm}$ or maximal 3 orders of magnitude relative to the reflectance value at $\rho = 1\,\mathrm{mm}$ the function $h(\rho) = a + b \cdot \rho + c \cdot \rho^2 + d \cdot \rho^{0.5}$ was fitted to the logarithmic SRR curves. (We remark that this function $h(\rho)$ was found empirically and later used for the calculations of the first and second derivative.) Thus $\tilde{R}(\rho)$ denotes the fitted, logarithmic SRR curve. At $\rho = 23\,\mathrm{mm}$ some SRR curves only reach a decrease of about 2.4 orders of magnitude relative to $\tilde{R}(1.2\,\mathrm{mm})$. This has to be taken into account during the evaluation of the SRR curves. A few logarithmic SRR curves are shown in figure 1a) and 3 chosen radial distances are marked. The radial distance at $\tilde{R}(1.2\,\mathrm{mm})$ was denoted ρ^+. The radial distance ρ^O (ρ^*) characterizes the radial distance where the SRR curve decreased 0.75 (2.4) orders of magnitude relative to $\tilde{R}(\rho^+)$. Correlations between the first derivative at ρ^* and the second derivative at ρ^O of the SRR curve and the OP were found. The first correlation between the curvature $\tilde{R}''(\rho^O) = \mathrm{d}^2(\tilde{R}(\rho))/\mathrm{d}(\rho)^2|_{\rho=\rho^O}$ of the SRR curve at ρ^O (see (O) in figure 1a)) and μ_s' is shown in figure 1b) for 1000 SRR curves. The empirically found function $f(\mu_s') = a + b \cdot \mu_s' + c \cdot (\mu_s')^3 + d \cdot e^{\mu_s'} + e \cdot \ln\mu_s'$ represents this correlation. It can be seen that the correlation is almost independent of μ_a. The second correlation is depicted in figure 2a). It shows the slope $\tilde{R}'(\rho^*) = \mathrm{d}\tilde{R}(\rho)/\mathrm{d}\rho|_{\rho=\rho^*}$

of the SRR curve at ρ^* (see (*) in figure 1a)) for different μ_s' that is plotted versus μ_a. We found that the ratio between the same μ_a values of two curves correlates with their reduced scattering coefficients, namely $\tilde{R}'(\rho^*_{c_1,j})/\tilde{R}'(\rho^*_{c_2,j}) = (\mu'_{s,c_1}/\mu'_{s,c_2})^{0.5}$. The indices c_1, c_2 stand for two different curves of μ_s' and $j = 1 \ldots 41$ for the different μ_a values. This correlation was considered while plotting the slope $\tilde{R}'(\rho^*)$ for 1000 SRR curves. Therefore $\tilde{R}'(\rho^*)$ for each of the 1000 SRR curves was multiplied by ${\mu_s'}^{-0.5}$. The result can be seen in figure 2b) and the correlation is represented with the function $g(\mu_a) = a + b \cdot \mu_a + c \cdot (\mu_a)^{-1} + d \cdot (\mu_a)^{-2}$, that was also found empirically.
We have chosen 2.4 orders of magnitude relative to $\tilde{R}(\rho^+)$ for the calculation of the slope since the slope at larger distances describes μ_a better. We found empirically that it is suitable to calculate the curvature at a decrease of 0.75 orders of magnitude relative to $\tilde{R}(\rho^+)$. To this end we changed the orders of magnitude between 0.7 and 0.9 as well as the reference point of the reflectance with $\rho = 1; 1.1; 1.2\,\mathrm{mm}$ for the same 1000 SRR curves as above. Using the function $f(\mu_s')$ the OP of two unknown testing datasets each consisting of about 1000 SRR curves were calculated and the combination with the best results was used for the evaluation.

3. Calculation of the optical properties

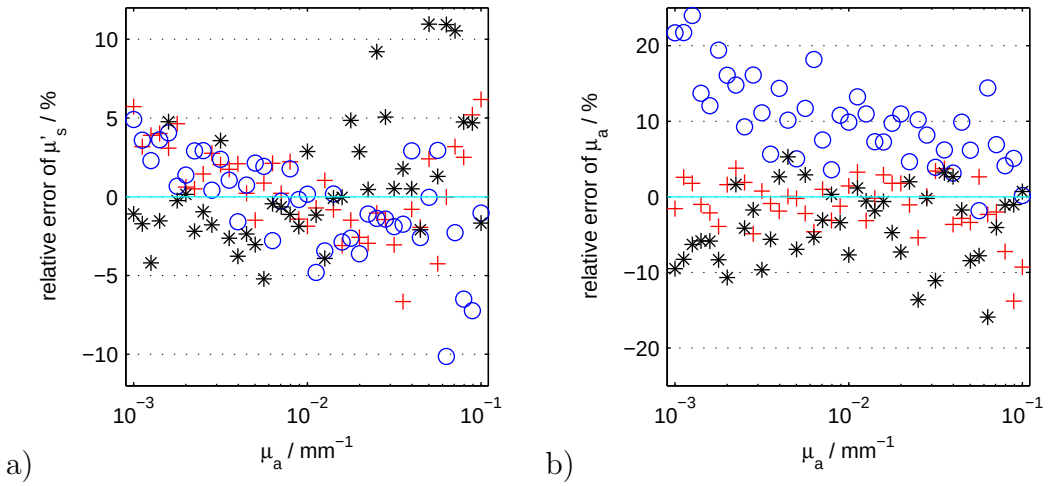

Figure 3. The relative errors of a) μ_s' and b) μ_a for $\mu_s' = 1\,\mathrm{mm}^{-1}$ (+), $\mu_s' = 2\,\mathrm{mm}^{-1}$ (O) and $\mu_s' = 4\,\mathrm{mm}^{-1}$ (*).

For the testing of our method 410 SRR curves with OP out of the range $0.5\,\mathrm{mm}^{-1} < \mu_s' < 5\,\mathrm{mm}^{-1}$ in $0.5\,\mathrm{mm}^{-1}$ steps and $0.001\,\mathrm{mm}^{-1} < \mu_a < 0.1\,\mathrm{mm}^{-1}$ in 40 equal steps in the logarithmic scale were simulated using MC simulations considering the setup geometry of our experimental arrangement as well as the noise that is characteristic for our measurement data. Applying the above explained correlations shown in figures 1b) and 2b) the OP were calculated. In the first step μ_s' was determined from the curvature at ρ^O. Knowing the determined μ_s', we calculated in the second step μ_a using the slope

at ρ^*. The relative errors for μ_s' and μ_a are depicted in figures 3a) and b) for 3 chosen μ_s'. It can be seen that μ_a is systematically determined too high ($\approx$10 %) for $\mu_s' = 2\,\mathrm{mm}^{-1}$ and too low ($\approx$4 %) for $\mu_s' = 4\,\mathrm{mm}^{-1}$. Whereas μ_s' can be determined without systematic errors. The average relative errors for all 410 SRR curves were 3.3 % and 8.7 % for μ_s' and μ_a, respectively.

4. Determination of the optical properties using an ANN

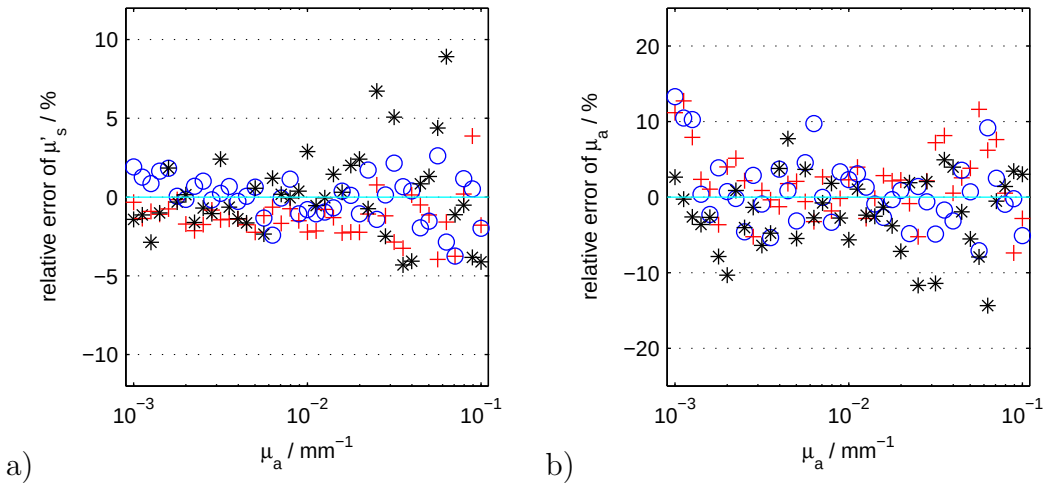

Figure 4. The relative errors of a) μ_s' and b) μ_a for $\mu_s' = 1\,\mathrm{mm}^{-1}$ (+), $\mu_s' = 2\,\mathrm{mm}^{-1}$ (O) and $\mu_s' = 4\,\mathrm{mm}^{-1}$ (*) obtained with the ANN.

An ANN containing 3 layers was also used for the determination of the OP from the slope and the curvature of the SRR curve. The curvature at ρ^O, the slope at ρ^* and the radial distances ρ^O and ρ^* were used as input values for the ANN. These 4 input values as well as the 2 output values (μ_s' and μ_a) were scaled within the range of 0.1 and 0.9 using $v_{sc} = [(v - v_{min})/(v_{max} - v_{min})] \cdot 0.8 + 0.1$. Here v_{sc} denotes the scaled value, v the original value and v_{min} and v_{min} the minimal and maximal occurring values. The hidden layer contains 11 hidden nodes. The principles of the applied ANN were similar to those explained by Boone *et al* 1990. The ANN was trained, validated and tested as explained previously (Jäger *et al* 2013) using a training, validating and testing dataset each consisting of 100 SRR curves. The weights that had the smallest error of the validation dataset were applied for the calculation of the OP of the testing dataset and any other unknown dataset. We performed 10^7 iterations but with 10^6 iterations almost the same result for the 410 systematic SRR curves can be achieved. The results for the same 410 systematic SRR curves as above are shown in figures 4a) and b). The average relative errors were 2.1 % and 4.4 % for μ_s' and μ_a, respectively. In comparison to the above method (see section 3) the results improved when an ANN was additionally used for the determination of the OP. We remark that no systematic errors could be seen while using an ANN.

In comparison the performance of an ANN that was not trained with the correlations between the derivatives and the OP was investigated as previously explained by Jäger *et al* 2013. It consisted of 3 layers with 11 input neurons that contain the radial distances corresponding to an equidistant decrease in the logarithm of the reflectance, 11 hidden neurons and 2 output neurons. Almost the same results as shown in figures 4a) and b) can be achieved but additional iterations during the learning process are necessary. We remark, in addition, that during the learning process more computation cost is needed because of the larger amount of input values (11 input values were used instead of 4). Furthermore, fewer input values speed up the executing phase, i.e. the determination of the OP of turbid media from unknown SRR curves. We note that it even takes more time to obtain the 11 input values since we first have to proceed our SRR curves to relative curves as explained in Jäger *et al* 2013.

5. Conclusion

A method for the determination of the OP of turbid media from simulated SRR curves that is valid for relative as well as absolute reflectance data is reported. We showed correlations between the curvature and the slope of the SRR curve and the reduced scattering and absorption coefficients, respectively. First these correlations (see figures 1b) and 2b)) were utilized for the calculation of the OP of unknown SRR curves. The average relative errors were 3.3 % and 8.7 % for μ_s' and for μ_a, respectively. Second, an ANN that was trained with 4 input values (curvature at ρ^O, slope at ρ^* and the radial distances ρ^O and ρ^* as shown in figures 1b), 2a) and 1a)) was investigated. Additionally, applying an ANN for the determination of the OP of turbid media from slope and curvature of the SRR curve improved the results for the unknown SRR curves. An average relative error of 2.1 % and 4.4 % was obtained for μ_s' and for μ_a, respectively. Applying an ANN that was trained with the correlations between the derivatives and the OP allows a fast determination of the OP of tissue from SRR curves. We used MC simulations that represented the geometry of our experimental arrangement as well as the noise characteristic of the measurement data. This enables the determination of the OP of turbid media from measured SRR curves. Since fewer input values accelerate the executing phase of the ANN our method is suitable for real-time measurement of the OP of tissue from SRR curves.

Acknowledgments

M. Jäger was financially supported by a post gradual PhD scholarship granted by Ulm University.

References

Boone J M, Sigillito V G and Shaber G S 1990 Neural networks in radiology: An introduction and evaluation in a signal detection task *Med. Phys.* **17** 234-241

Farrell T J, Wilson B C and Patterson M S 1992 The use of a neural network to determine tissue optical properties from spatially resolved diffuse reflectance measurements *Phys. Med. Biol.* **37** 2281-2286

Foschum F, Jäger M and Kienle A 2011 Fully automated spatially resolved reflectance spectrometer for the determination of the absorption and scattering in turbid media *Rev. Sci. Instrum.* **82** 103104

Foschum F and Kienle A 2013 An optimized goniometer for determination of the scattering phase function of suspended particles - simulations and measurements *J. Biomed. Opt.* **18** 085002

Jäger M and Kienle A 2011 Non-invasive determination of the absorption coefficient of the brain from time-resolved reflectance using a neural network *Phys. Med. Biol.* **56** N139–N144

Jäger M, Foschum F and Kienle A 2013 Application of multiple artificial neural networks for the determination of the optical properties of turbid media *J. Biomed. Opt.* **18** 057005

Kanick, S C and Gamm, U A and Schouten, M and Sterenborg, H J C M and Robinson, D J and Amelink, A 2011 Measurement of the reduced scattering coefficient of turbid media using single fiber reflectance spectroscopy: fiber diameter and phase function dependence *Biomed. Opt. Express* **2** 1687–1702

Kienle A, Lilge L, Patterson M S, Hibst R, Steiner R and Wilson B C 1996 Spatially resolved absolute diffuse reflectance measurements for noninvasive determination of the optical scattering and absorption coefficients of biological tissue *Appl. Opt.* **35** 2304–2314

Martelli, F and Zaccanti, G 2007 Calibration of scattering and absorption properties of a liquid diffusive medium at NIR wavelengths. CW method *Opt. Express* **15** 486–500

Pfefer T J, Matchette L S, Bennett C L, Gall J A, Wilke J N, Durkin A J and Ediger M N 2003 Reflectance-based determination of optical properties in highly attenuating tissue *J. Biomed. Opt.* **8** 206–215

Wang L H, Zhao X M and Jacques S L 1994 Computation of the optical properties of tissues from light reflectance using a neural network *Proc. SPIE* **2134A** 391–399

Wang Q, Shastri K and Pfefer T J 2010 Experimental and theoretical evaluation of a fiber-optic approach for optical property measurement in layered epithelial tissue *Appl. Opt.* **49** 5309–5320

Warncke D, Lewis E, Lochmann S and Leahy M 2009 A neural network based approach for determination of optical scattering and absorption coefficients of biological tissue *JPCS* **178** 012047

Chen Y, Lin L, Li G, Ye W and Yu Q 2003 Determination of tissue optical properties from spatially resolved relative diffuse reflectance by PCA-NN *IEEE ICNNSP* **1** 369–372

Zhang L, Wang Z and Zhou M 2010 Determination of the optical coefficients of biological tissue by neural network," *J. Mod. Opt.* **57** 1163–1170